Since January 2020 Elsevier has created a COVID-19 resource centre with free information in English and Mandarin on the novel coronavirus COVID-19. The COVID-19 resource centre is hosted on Elsevier Connect, the company's public news and information website.

Building and Environment 186 (2020) 107373

Contents lists available at ScienceDirect

Building and Environment

journal homepage: http://www.elsevier.com/locate/buildenv

Full-scale experimental and numerical study of bioaerosol characteristics against cross-infection in a two-bed hospital ward

Zhijian Liu [a,*], Liangqi Wang [a], Rui Rong [a], Shifeng Fu [c], Guoqing Cao [b], Cuicai Hao [c]

[a] Department of Power Engineering, North China Electric Power University, Baoding, Hebei, 071003, PR China
[b] Institute of Building Environment and Energy, China Academy of Building Research, Beijing, 100013, PR China
[c] Hebei Academy of Building Research Co,Ltd, Shijiazhuang, Hebei, 050031, PR China

ARTICLE INFO

Keywords:
Full-scale experiment
Hospital ward
Bioaerosol
Air distribution
Airborne transmission

ABSTRACT

The transmission and deposition of pathogenic bioaerosols and the subsequent contamination of the air and surfaces is well recognized as a potential route of hospital cross-infection. A full-scale experiment using *Bacillus subtilis* and computational fluid dynamics were utilized to model the bioaerosol characteristics in a two-bed hospital ward with a constant air change rate (12 ACH). The results indicated that the bioaerosol removal efficiency of unilateral downward ventilation was 50% higher than that of bilateral downward ventilation. Additionally, health care workers (HCWs) and nearby patients had lower breathing zone concentrations in the ward with unilateral downward ventilation. Furthermore, a partition played a positive role in protecting patients by reducing the amount of bioaerosol exposure. However, no obvious protective effect was observed with respect to the HCWs. Only 10% of the bioaerosol was deposited on the surfaces in the ward with unilateral downward ventilation, while up to 35% of the bioaerosol was deposited on the surfaces in the ward with bilateral downward ventilation during the 900 s. The main deposition locations of the bioaerosols were near the wall on the same side of the room as the patient's head in all cases. This study could provide scientific evidence for controlling cross-infection in hospital wards, as well as several guidelines for the disinfection of hospital wards.

1. Introduction

With the worldwide emergence of COVID-19 this year, a significant number of infected patients are being admitted to hospitals, and front-line medical staff are subsequently being infected. In recent years, with continual outbreaks of severe acute respiratory syndrome (SARS), Middle East respiratory syndrome (MERS), tuberculosis and other new infectious diseases, airborne diseases are receiving increased attention globally [1]. The process of bioaerosol particles (e.g., viruses, bacteria, and fungi) releasing and spreading through the air is one of the main transmission routes of infection [2]. The outbreak of airborne diseases in hospitals increases the risk of infection from patients to health care workers (HCWs) and other patients. As such, the purpose of a mechanical ventilation system (with both air supply and exhaust devices) is to control the airflow to protect other patients and HCWs from contamination by infected patients. An effective mechanical ventilation design is important in reducing the spread of airborne diseases in hospital isolation rooms [3,4].

There are specifications and guidelines in place that provide standards for the design of airflow organization for use in infectious wards. The Centers for Disease Control and Prevention recommends that a once-through ventilation system is preferable in areas where infectious droplet nuclei may exist [5]. Australia recommends uniform air supply vents on the ceiling and multiple exhaust vents on the lower walls. China stipulates that the air inlet of a negative pressure isolation ward should be placed in the upper part of the room, while the exhaust vent should be placed near the patient's head. In general, the purpose of these standards is to form a unidirectional airflow pattern so that pollutants can be removed quickly while simultaneously protecting the HCWs.

Meanwhile, a series of studies have used visualization technology and computational fluid dynamics (CFD) simulation to study the design of airflow organization and the effectiveness of ventilation in hospital wards. Tang et al. used the human body model and visualization technology to observe and study the characteristics of human respiratory activity so that the air movement carrying infectious materials could be intuitionistic and quantified in time and space [6]. Research on the spread of viruses through the air has also been conducted in hospital environments, with an emphasis on the analysis of the spread of

* Corresponding author.
E-mail address: zhijianliu@ncepu.edu.cn (Z. Liu).

https://doi.org/10.1016/j.buildenv.2020.107373
Received 9 August 2020; Received in revised form 21 September 2020; Accepted 10 October 2020
Available online 12 October 2020

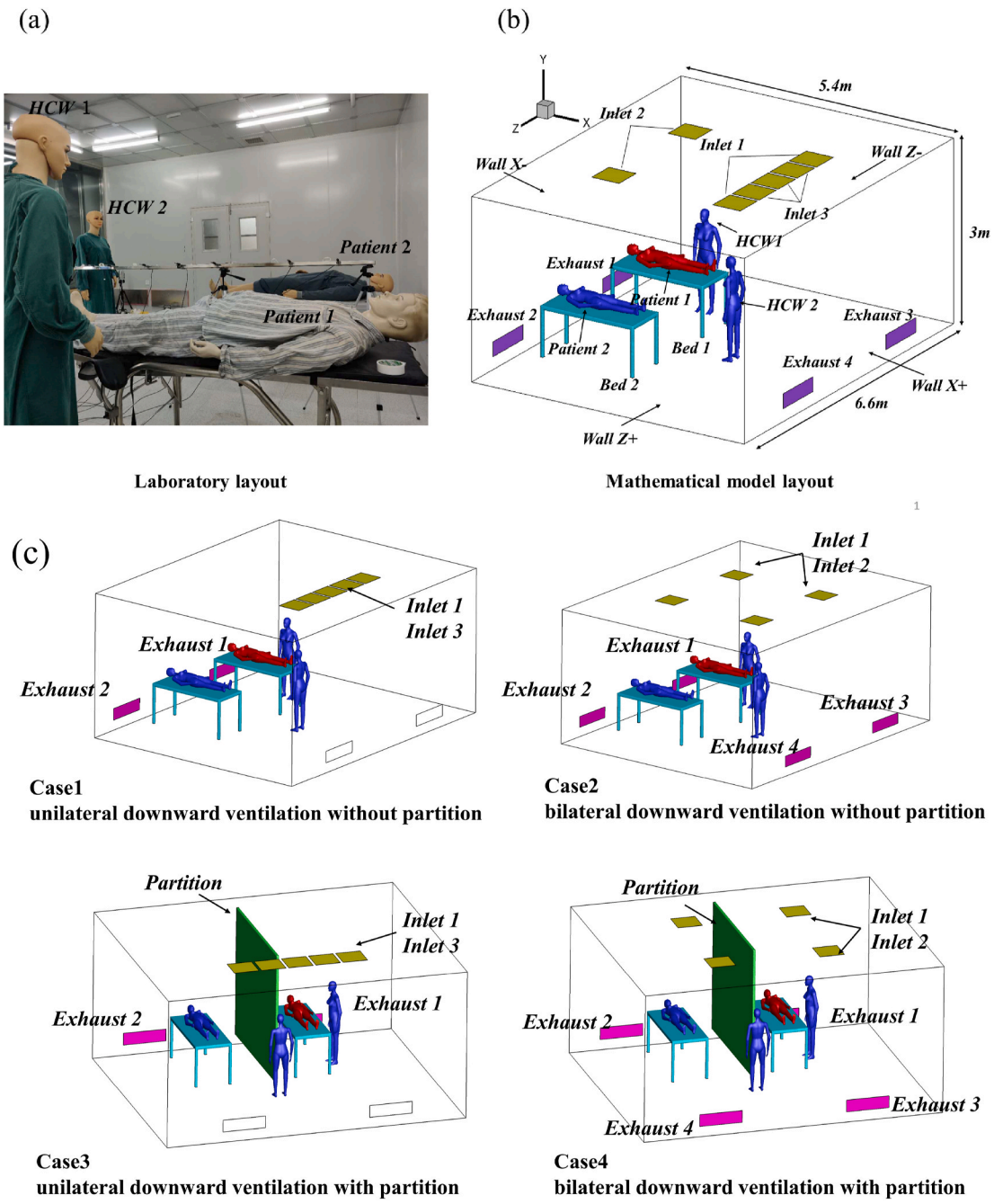

Fig. 1. (a) Laboratory layout; (b) mathematical model layout; and (c) layouts for Cases 1–4.

pathogenic microorganisms. Several studies have used tracer gas simulation to analyze the path of infection during an outbreak in a hospital, and they were able to confirm the airborne transmission of a virus between the first infected patient and a newly infected person by checking the changes in concentration of the tracer gas [7–10]. Cheong et al. investigated the influence of three different ventilation types on the distribution of pollutants in hospital wards. The results showed that the ventilation of the upper air supply and lower air return on both sides of the hospital bed had the best pollutant removal effect [11]. Because of the locations of the supply air, return air, and exhaust air, the risk of viruses spreading through the hospital was influenced by the changes in the movement and direction of the airflow. In rooms with mixed ventilation and downward ventilation, the pollutants were almost completely mixed in the occupied area and removed by the dilution process [12–15]. Displacement ventilation has been considered an effective and widely used method to control air quality in common indoor environments. However, in a hospital isolation ward, whether displacement ventilation could better remove pollutants in the breathing zone was dependent upon the location of the exhaust vent [16,17]. Qian et al. studied the effectiveness of a downward ventilation system in a hospital ward; the results showed that when the air change rate was 4 h-1, the heat plume generated by a human body was mixed with supply air, and unidirectional airflow could not be formed. It was recommended that an investigation of a ventilation system with different air diffuser and exhaust locations should be conducted to determine if the risk of infection could be reduced [18]. Nielsen et al. studied a downward air supply system with a low-speed diffuser on the ceiling. The location of the exhaust played an important role in the removal of pollutants (i.e., tracer gas) in the room. When viruses or bacteria spread in the air (<5 μm), a low exhaust location did not cause an exposure index of greater

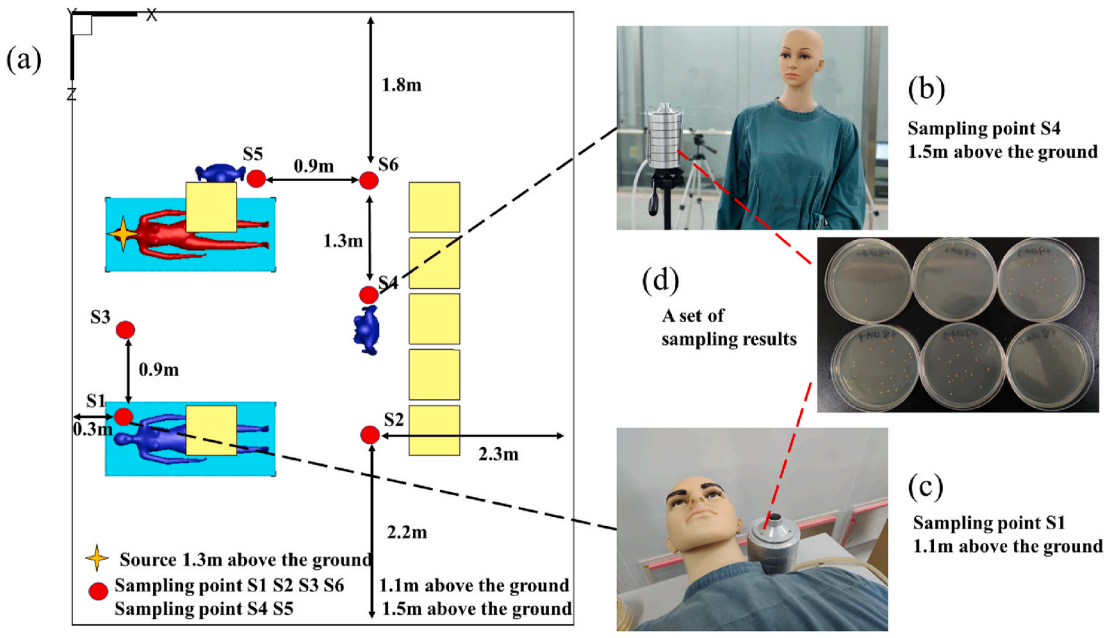

Fig. 2. Locations of sampling points in bioaerosol experiment.

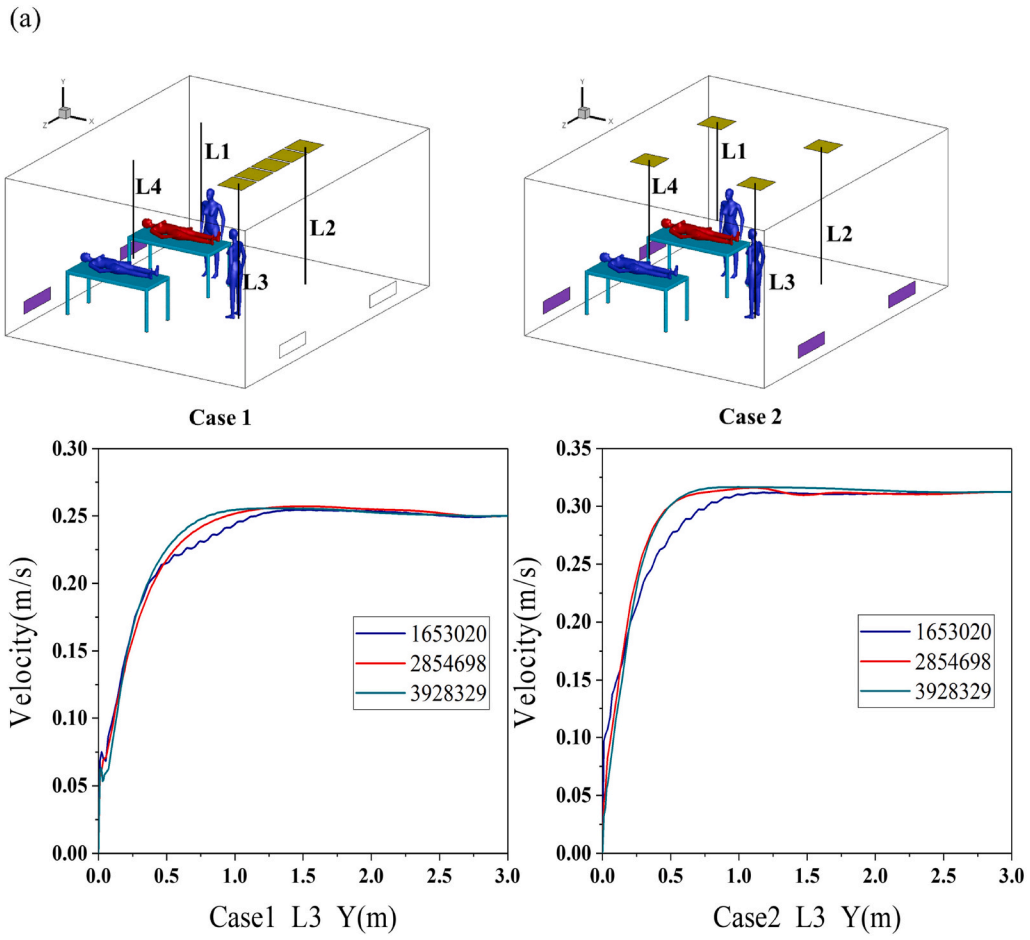

Fig. 3. (a) Measuring points of air velocity and (b) grid independence verification.

than 1.0 for patients in wards with this type of ventilation system [15]. Overall, downward ventilation has been the most effective form of air supply in hospital wards to date.

Contact transmission risk caused by bioaerosol deposition has also been an important factor to consider when evaluating the occurrence of cross-infection in hospital wards. The deposition of particles (0.01–10

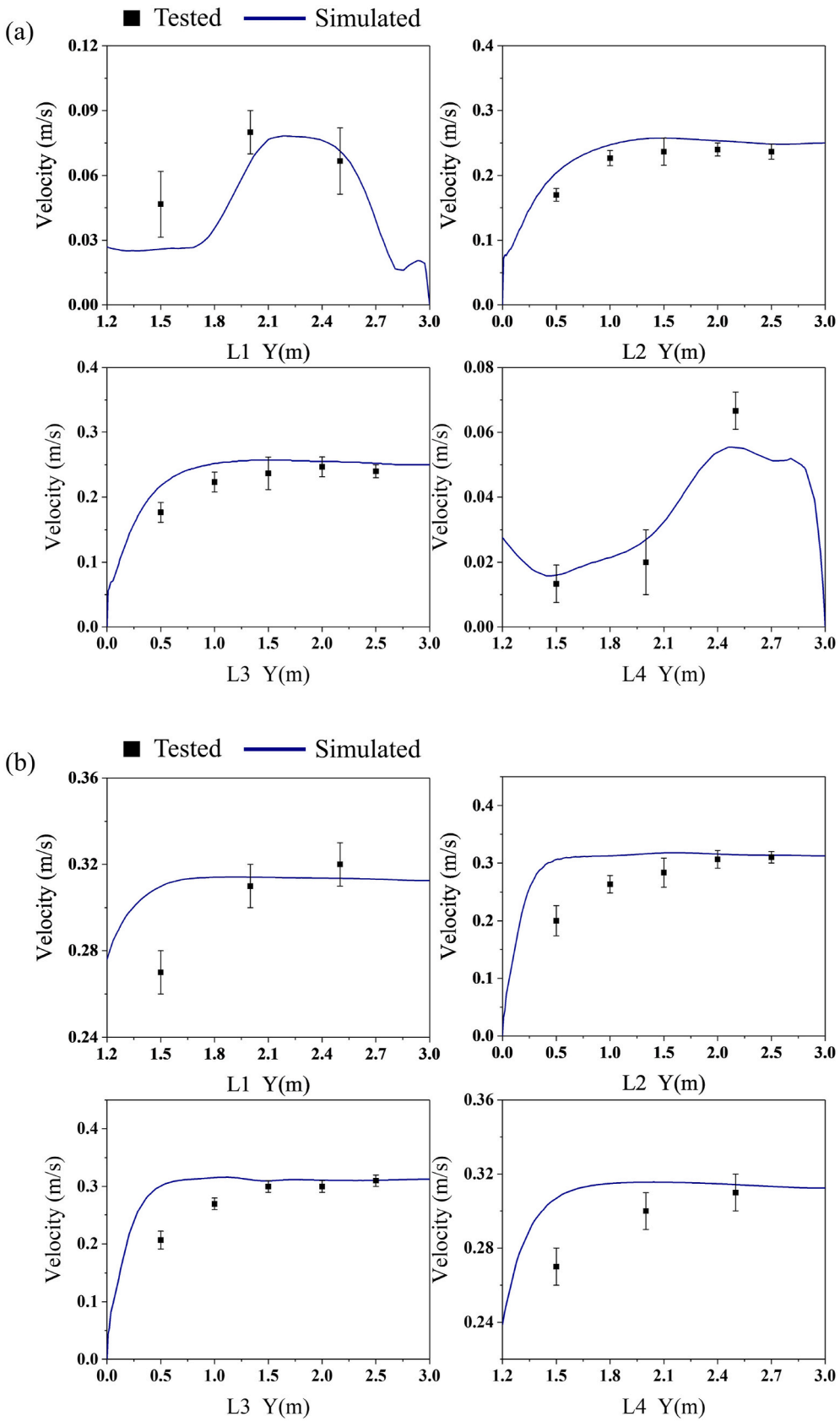

Fig. 4. Comparison of experimental and simulated values of airflow velocity.

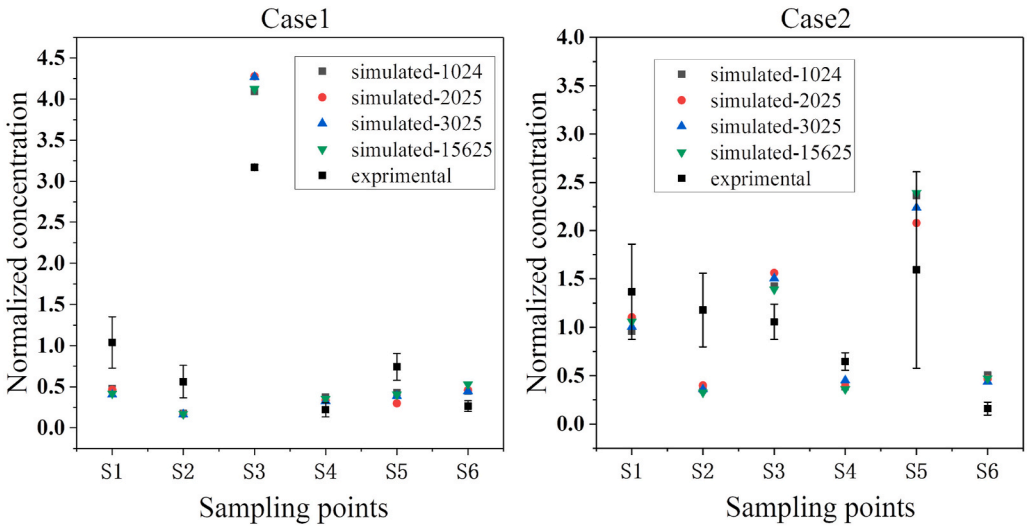

Fig. 5. Comparison of experimental and simulated values of normalized concentrations.

μm in size) was predicted by Lai and Chen, and there was strong evidence that larger particles were deposited near the release source and that they did not remain suspended [19,20]. King et al. proved that bioaerosols with diameters less than 5 μm were deposited on indoor surfaces; however, the relationship between the surface concentration and distance from the release source was not obvious [21]. Meanwhile, it was found that a partition played a role in the risk of cross-infection between two patients [22]. Many hospitals lack sufficient single-patient rooms because of restrictions in the construction area. Therefore, to reduce the risk of cross-infection caused by bioaerosols in two-bed rooms, it was necessary to explore the actual effect of partitions.

All the aforementioned studies have highlighted the need to achieve better pollutant removal efficiency in hospital wards. However, these studies have only focused on the effect of removing indoor pollutants under different ventilation conditions and airflow patterns, which has not been sufficient. As Hathway et al. emphasized, there are few direct comparisons between CFD models and bioaerosol experiments [1]. To create a significantly safer environment for HCWs and nearby patients, additional research should be conducted to determine improved methods of bioaerosol removal, as well as the characteristics of a typical two-bed ward layout with respect to time and space. Therefore, the purpose of this study was to determine ventilation efficiency and to confirm which locations had the most significant bioaerosol deposition within a typical two-bed ward layout to provide recommendations for the protection of HCWs and nearby patients. A full-scale experiment and CFD methods were used to explore the bioaerosol characteristics in a typical two-bed hospital room. The ventilation efficiency for the removal of bioaerosols was quantitatively examined in a ward with two types of typical downward ventilation. The temporal and spatial distributions of bioaerosols in four different cases (or scenarios) were determined. The time-varying breathing zone concentrations of the HCWs and nearby patients were also quantitatively analyzed. Additionally, the effectiveness of partitions in limiting the spread of bioaerosols in a hospital ward was explored. Our results will provide scientific recommendations for the protective effects of ventilation measures on HCWs, as well as suggestions for optimizing the air distribution in hospitals. Furthermore, our results will help to effectively control the spread of bioaerosols in wards, as well as reduce the risk of cross-infection in hospitals.

2. Experimental method

2.1. Experimental setup

This study was conducted in a typical environmentally controlled laboratory in Beijing. The size of the two-bed ward in the experiment was similar in size to that of a standard hospital room: length (L) × width (W) × height (H) = 6.6 m × 5.4 m × 3 m. External air was supplied by a fan filter unit at the top of the chamber, and it was HEPA-filtered before being directed to the room. The experimental room was arranged in a typical ward layout: two beds, two patient mannequins, and two mannequins representing HCWs, which was similar to the setup in the study conducted by Qian et al. [18]. The temperature and relative humidity in the experimental room were 20.1 °C and 39.5%, respectively. The dimensions of the beds were each 1.8 m (L) × 0.8 m (W) × 0.83 m (H). With respect to subsequent wall deposition, the name of each wall was simplified; X- and Z-represented the two side walls closest to the pollution source, and X+ and Z+ represented the two side walls away from the pollution source. Fig. 1(a) and (b) show the specific layout of the experimental room.

The size of the air supply orifice at the top of the room was 0.54 m × 0.54 m, and the size of the high-efficiency air outlet was 0.984 m × 0286 m. The ventilation rate was maintained at approximately 12 ACH in all experimental scenarios. Two types of downward ventilation with floor exhaust were arranged based on the specific conditions of the laboratory. Four cases were arranged in this study, as shown in Fig. 1(c). Case1 was unilateral downward ventilation without partition. Case2 was bilateral downward ventilation without partition. Case3 was unilateral downward ventilation with partition. Case4 was bilateral downward ventilation with partition. The partition was positioned 20 cm above the floor and 20 cm below the ceiling like the setup of King et al. [21]. The inlet air velocity of the unilateral downward ventilation was 0.25 m/s, while that of the bilateral downward ventilation was 0.31 m/s.

Hot-wire anemometers were used to determine the air velocity of the ward (with two types of downward ventilation) prior to the bioaerosol experiment. Four vertical measuring lines under inlets 1 and 2 were selected to measure the air velocity. The positions of the measuring lines are shown in Fig. 3(a), and the measuring points were arranged every 0.5 m. The indoor air velocity measurement results were then used to generate boundary conditions and to verify the simulated results.

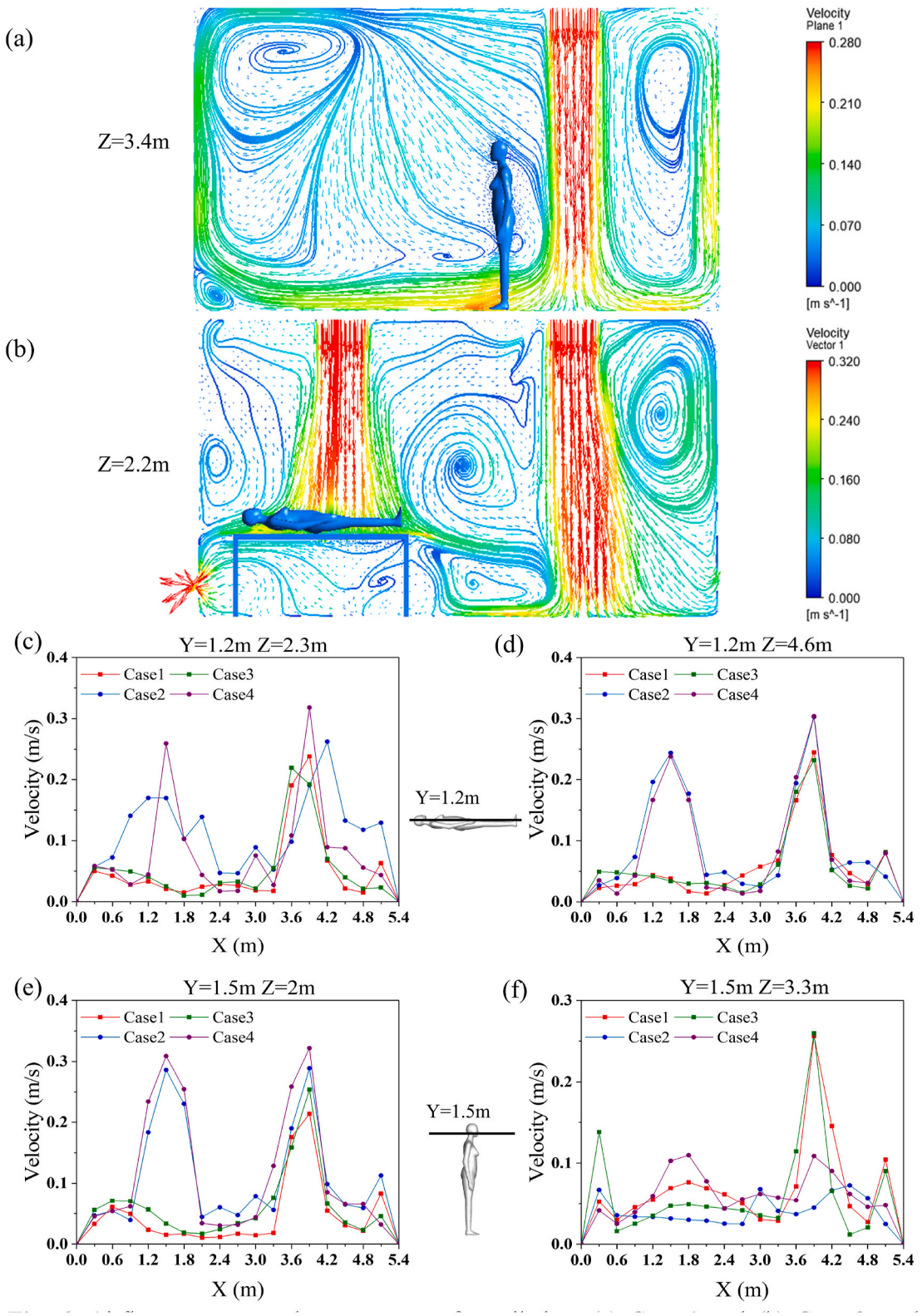

Fig. 6. Airflow patterns under two types of ventilation: (a) Case 1 and (b) Case 2; and breathing zone air velocities of humans in ward: (c) patient 1, (d) patient 2, (e) health care worker 1 (HCW1), and (f) health care worker 2 (HCW2).

2.2. Bioaerosol experiment

The Gram-positive bacterium, *Bacillus subtilis*, was the strain used in this experiment. After being cultured, this strain showed an orange colony color, which could be distinguished from the miscellaneous bacteria in the air. This strain was not harmful to the experimental personnel, and the particle size and density were representative.

The suspension of *Bacillus subtilis* was diluted, and the concentration of the diluted suspension was 5.81×10^6 CFU/ml. The diluted bacterial suspension was released in the laboratory through a Laskin nozzle. The

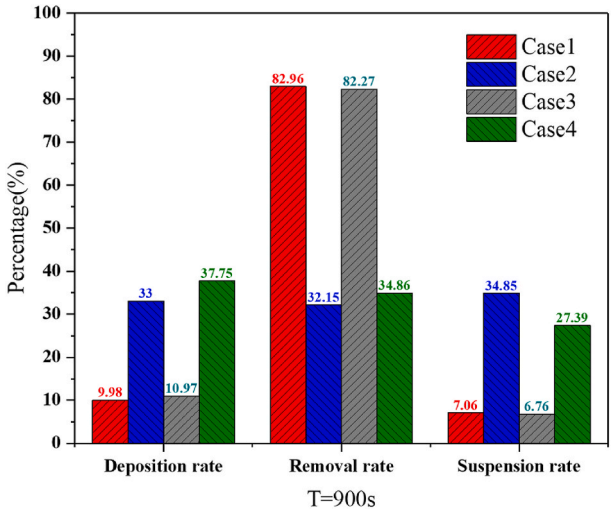

Fig. 7. Deposition, removal, and suspension rates of the four cases during 900 s.

nozzle was equipped with a separate air pump and flowmeter, and the air filtered by the high-efficiency filter entered the nozzle at a rate of 10 L/min. The density of the bioaerosol produced by the Laskin nozzle was 1000 kg/m^3, which is approximately equal to the density of water. The size of the bioaerosol was 1–5 μm and had a mass median diameter of 2.5 μm. The release position was above the head of patient 1, 1.3 m from the floor. Simultaneously, six bioaerosol sampling points (S1–S6) were arranged around the work area of the ward, and the specific locations are shown in Fig. 2. The source of release was set at patient 1, 1.3 m above the floor. The direction of release was blowing upward. S1, S2, S3, and S6 were set at 1.1 m above the floor, while S4 and S5 were set at 1.5 m above the floor.

After measuring the background concentration of *Bacillus subtilis* in the room, a bioaerosol release experiment was conducted. In this experiment, after turning on the air supply system and the bioaerosol generator for 10 min, the bioaerosol samplers at the six measuring points were turned on. The sampling flow rate was 28.3 L/min through an Andersen six-stage sampler, and the time at each sampling point was 5 min. The experiments were conducted in triplicate for each of the four cases. The sampled media were cultured in a constant temperature incubator for 24 h.

2.3. Error analysis

The Andersen six-stage sampler was used to sample the indoor bacteria, which is one of the most effective ways to sample indoor culturable bacteria [23]. The Andersen sampler counted the colony forming unit (CFU) in each Petri dish, which was expressed as CFU per cubic meter of air (CFU/m^3). However, because of the overlay of colonies when the bioaerosols hit the container through the same sieve holes, the sampling number of colonies at all levels can be modified by Eq. (1). Then, Eq. (2) can be used to calculate the concentration of culturable bacteria in the air [24].

$$Pr_i = N_i\left(\frac{1}{N_i}+\frac{1}{N_i-1}+\frac{1}{N_i-2}+\cdots\frac{1}{N_i-r_i+1}\right) \tag{1}$$

$$C\left(CFU\,/\,m^3\right)=\frac{\sum_{i=1}^{6}Pr_i\times 1000}{T(min)\times F(L/min)} \tag{2}$$

where C is the concentration of culturable bacteria in the air, N_i is the number of sieve holes of class I of the sampler, r_i is the number of colonies of class i, Pr$_i$ is the number of colonies after class I modification, T is the sampling time, and F is the sampling rate.

3. CFD methodology

3.1. Airflow phase simulation

The indoor airflow turbulent simulation can be simulated by three turbulence models: direct numerical simulation (DNS), large eddy simulation (LES), and Reynolds averaged Navier-Stokes (RANS). However, the DNS and LES models require more computer memory and longer calculation times in indoor airflow simulation [25,26]. The renormalization group (RNG) k–ε turbulence model in the RANS method is widely used in indoor airflow simulations and has proven effective within the RANS turbulence models [27]. The RNG k–ε model is one of the best turbulence models compared with those of other RANS methods, especially with respect to accuracy, computational speed, and stability of indoor environment modeling [28,29]. Therefore, the RNG k–ε turbulence model was adopted in this study. The standard wall function was used near the wall. The general form of the governing equation can be expressed as follows.

$$\frac{\partial(\rho\varphi)}{\partial t}+\nabla\cdot\left(\rho\varphi\,\overrightarrow{V}\right)=\nabla\cdot(\Gamma_\varphi\nabla\varphi)+S_\varphi \tag{3}$$

where ρ is the air density, $\overrightarrow{V}$ is the air velocity vector, φ represents each of the three velocity components, Γ_φ is the effective diffusion coefficient of φ, and S_φ is the source term.

For the boundary conditions, a velocity inlet was used for the supply air inlet, and outflow was used for the return air outlet. The finite volume method was used to discretize the conservation control equations. To improve the numerical accuracy, the constraint terms and diffusion constraint terms in the second-order upwind discrete control equation were adopted, and the flow field calculation method used the SIMPLE algorithm. The air parameters of fluent $\rho = 1.225$ kg/m^3 and $\mu = 1.84\times10^{-5}$ ns/m^2 were used in the airflow phase simulation.

3.2. Particle phase simulation

The motion of the particle phase was calculated by the Lagrangian particle tracking method, and the discrete random walk model was applied to simulate the dispersion of the particles due to turbulence. The bioaerosols were simulated as spherical particles with a density of 1000 kg/m^3 and a diameter of 2.5 μm, which was determined by the mass median diameter of the particles ejected from the nozzle. In this study, the steady state calculation of the airflow field in four cases was conducted, and then the particles were added for the transient state calculation. The sampling time of each group in the experiment was 15 min; therefore, in the transient numerical calculation, the time step was set to 1 s, and the total calculation time was 900 s. In this way, the relevant sampling point data could be accurately extracted for comparison and verification, and the diffusion law of bioaerosols could be fully tracked. Considering the airflow condition and the bioaerosol size released in this study, the Saffman lift force was calculated, and the additional forces were negligible in comparison with that of the resistance [30]. The equation is as follows.

$$\frac{du_{pi}}{dt}=\frac{18\mu}{\rho_p d_p^2}\frac{C_D Re}{24}\left(u_i-u_{pi}\right)+g_i\left(1-\frac{\rho}{\rho_p}\right)+F_{ai} \tag{4}$$

where u_i and u_{pi} are the instantaneous velocities of the fluid and particles, respectively; μ is the molecular viscosity of the fluid; ρ and ρ_p are the densities of the fluid and particles, respectively; d_p is the diameter of the particles; Re is the particle Reynolds number; C_D is the drag coefficient; g_i is the gravitational acceleration in the i direction; and F_{ai} is the additional force exerted on the particles.

After calculating the turbulent flow field, the particles were injected into the airflow domain. Specifically, when the particles reached the exhaust of the ward, they were considered to have left the area, and the

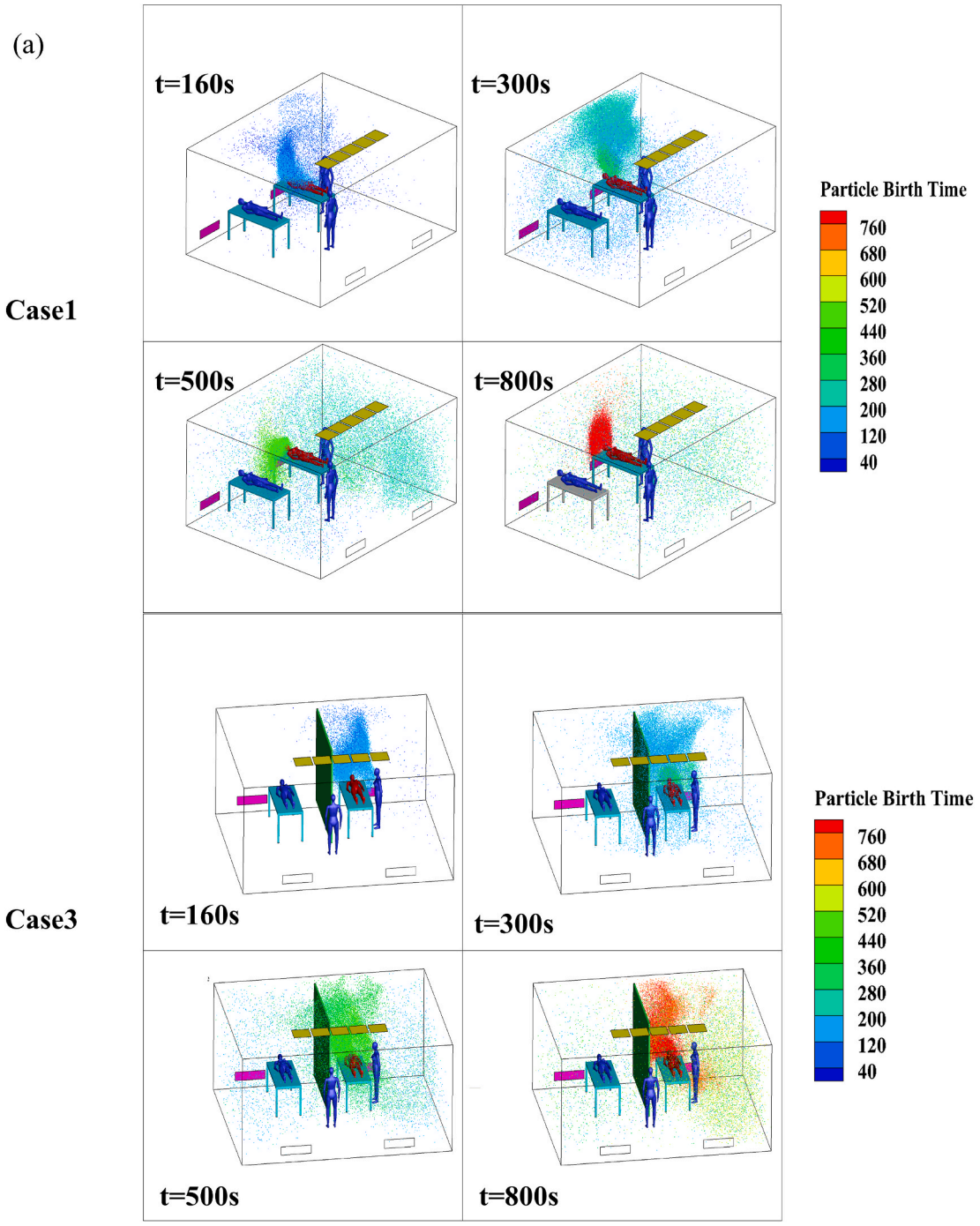

Fig. 8. Temporal and spatial distributions of bioaerosols in four cases.

exhaust was set to the escape condition. Meanwhile, it was assumed that the particles were captured after impacting a hard surface, and the wall was set to the trap boundary condition because particles cannot typically obtain enough rebound energy to resist adhesion. According to Hinds [31], because of the low solid content and short experimental time, the concentration of the particles will be halved owing to solidification. Thus, it was assumed that no solidification or collision between particles occurred and that the size of the particles did not change. The field measurement results showed that the temperature of the room was uniform and that the temperature difference between the air supply and air return was insignificant. Therefore, the influence the temperature difference had on the aerosol force and airflow was neglected in this model. The concentration in the simulation was converted based on the concentration of viable microorganisms obtained by Anderson sampler, so all particles in the simulation were assumed to be viable. In addition, the experiment and simulation time in this study was relatively short. The growth, reproduction and death characteristics of the bioaerosol diffusion process in the simulation could be neglected due to the short time in the air. This assumption was also used in the former reference [21]. According to Wei et al. [32], the evaporation time of small particles is very short, and the evaporation time of 2 μm particles is approximately 0.0025–0.027 s. A similar conclusion was drawn by Morawska [8]; therefore, the evaporation effect could be neglected in our simulation because of the small size of the selected bioaerosols.

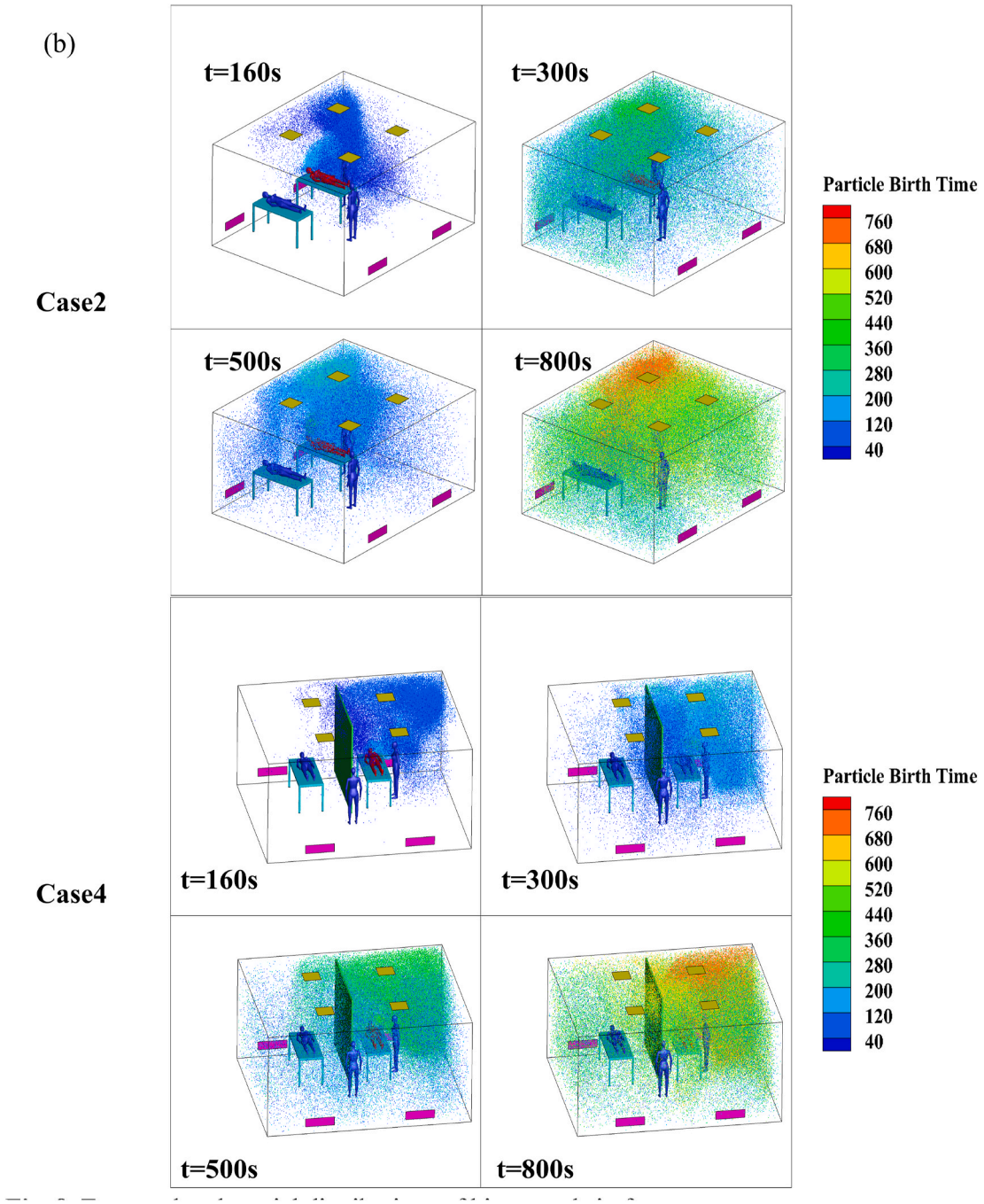

Fig. 8. (*continued*).

The particles were released from the same source location as the experimental setup. This study considered four different particle release rates (1024, 2025, 3025, and 15625 CFU/s) under two downward ventilation types to verify the sensitivity of the number of particles. As shown in Fig. 5, the normalized concentrations of the particles with the four different release rates were basically consistent at the sampling points. To ensure calculation accuracy and reduce the calculation amount, a rate of 1024 CFU/s was selected for the subsequent transient simulations.

3.3. Validation of numerical model

Mesh density and structure have significant effects on the airflow results [33,34]. In this study, CFD methods were used to test the grid independence of the aforementioned full-scale laboratory, and three sets of grids with the numbers of 1653020, 2,854,698, and 3,928,329 were generated and numerically simulated. All three types of meshes encrypted the human body surface and position with a large velocity gradient. The grid independence was verified on the vertical air velocity measurement line (L3) directly below the air supply outlet in two airflow patterns, and the results are shown in Fig. 3(b). The velocity change between the two sets of grids with the numbers of 2,854,698 and 3,928,329 was exceedingly small. Therefore, considering the accuracy and calculation amount, a grid with the number of 2,854,698 was selected for the subsequent simulations.

The main purpose of the airflow field verification in the ward was to verify the accuracy of the simulated results of the airflow phase. In this model, the movement of bioaerosols was most affected by the airflow;

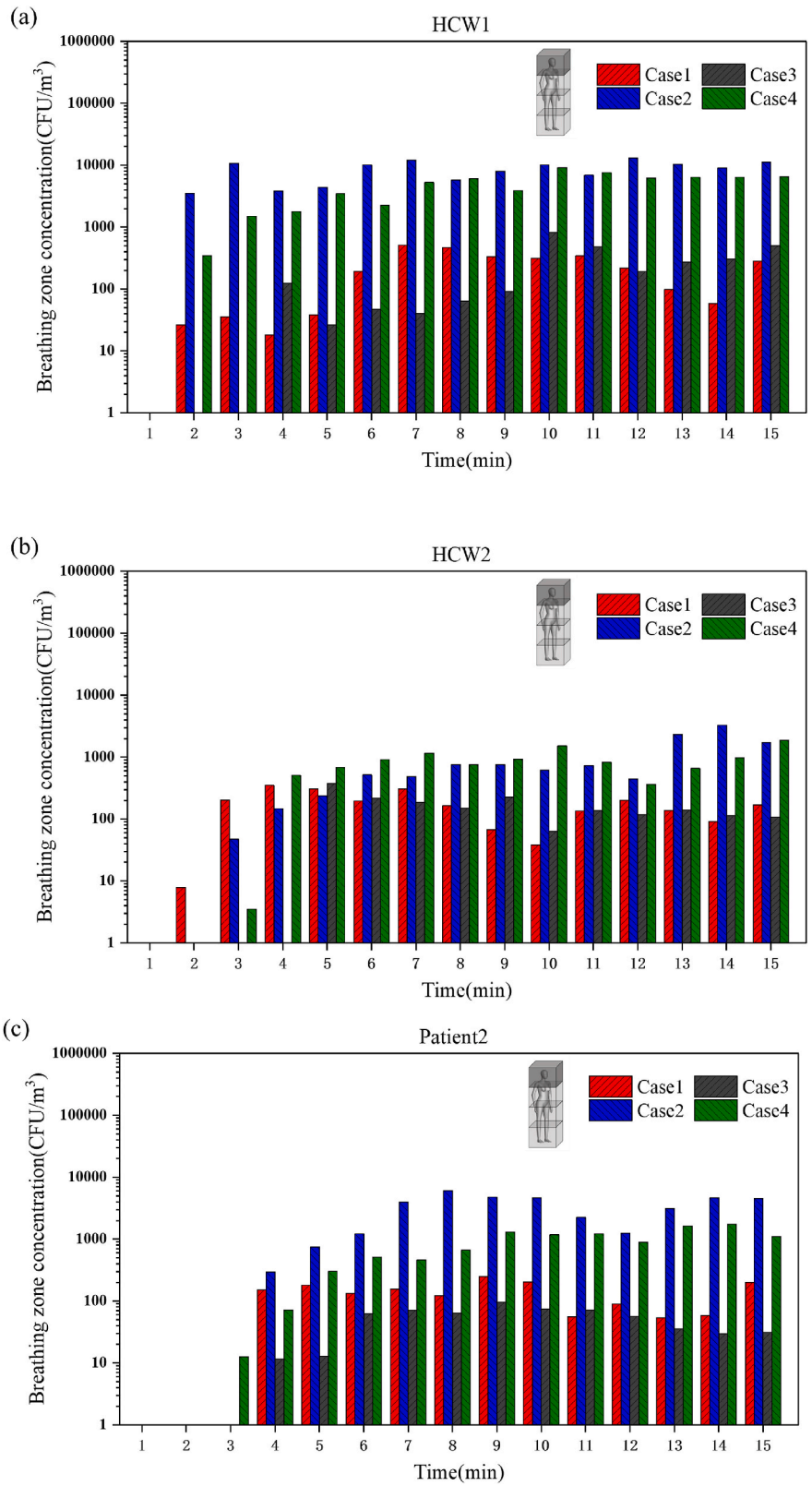

Fig. 9. Breathing zone concentrations of (a) HCW1, (b) HCW2, and (c) patient 2 during 900 s.

therefore, an accurate continuous phase calculation model was particularly important for the study of the distribution and diffusion of the bioaerosols. The verification of the airflow field was confirmed by the change in the air velocity directly under the four air inlets (inlet 1, inlet 2) with a change in height. The air velocity verification results of the two ventilation types are shown in Fig. 4(a) and (b). Results show that the experimental and numerical velocity data are basically consistent. The mean absolute percentage error (MAPE) for velocity was less than 10% [35], suggesting that the boundary condition settings of the flow field are reasonable. The error between the numerical simulation and the

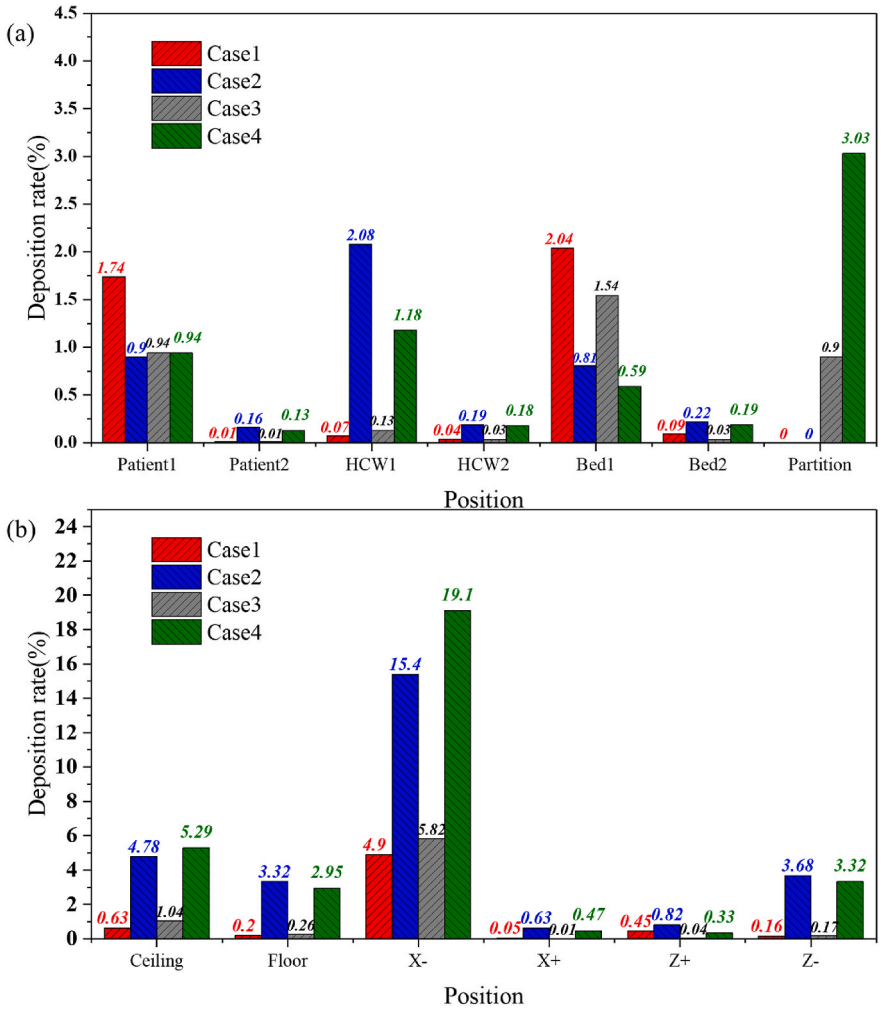

Fig. 10. Comparison of bioaerosol deposition rates on different surfaces in four cases: (a) beds, body surfaces, partition, and (b) indoor walls.

experimental results was due to the fact that the actual airflow field was turbulent, this meant it was difficult to collect the velocity parameters accurately by simply using anemometers. Anemometry measurements are invasive and disturb the flow to capture velocity. At the same time, the numerical simulation was also simplified for the air supply model and air medium, which would lead to certain errors; however, the errors were acceptable for the analysis of this model.

Fig. 5 shows the verification of the experimental results and simulated results of the bioaerosol concentrations at the six measurement points for the two types of downward ventilation. The experimental values and simulated values were processed and normalized, respectively. The average concentration of the six sampling points was used as the denominator of the experimental value, and the average value of the average concentration of the six sampling points after 5 min was taken as the denominator of the simulation value. The four groups of points and error bars in Fig. 5 represent the comparative trends of the simulated and measured concentrations of the bacterial aerosols at the six sampling points. The measured results from the two types of downward ventilation corresponded well with the simulated results. Although the results did not exactly correspond, considering the complexity of microbial sampling, a certain degree of deviation was expected, and the overall trend of each measurement point was not affected. Overall, the concentration verification showed that the model and experimental results achieved good consistency, which ensured the accuracy of subsequent simulations.

4. Results and discussion

4.1. Airflow pattern

Fig. 6(a) shows the streamline vector diagram of the center section of the ward with unilateral downward ventilation, as in Case 1. The split flow hit the front and rear walls to form a backflow after the vertical air was supplied to the floor. Then, a portion of the airflow moved up to the ceiling along the wall and formed an eddy current zone, while the other portion moved to the air supply area and returned. Fig. 6(b) shows the streamline vector diagram of the section, Z = 2.2 m, in the ward with bilateral downward ventilation. After the vertical air supply on the right side reached the floor, the split flow hit the rear wall and hospital bed to produce a reverse airflow. The airflow on the other side also formed an eddy current zone on the left side of bed 1.

Fig. 6(c), (d), (e), and (f) show the changes in the air velocity around the breathing zones of each person in the ward processed from the simulated results. The height of the breathing zone for patients 1 and 2 was set to 1.2 m, and the trend of the air velocity of the breathing zone in the X direction is shown in Fig. 6(c) and (d). The air velocity of patients 1 and 2 (within a distance of 0–2.4 m in the four cases) was kept below 0.2 m/s. When the partition was added in Cases 3 and 4, the changes in air velocity in the breathing zones were not obvious. Because the standing position of health care worker 1 (HCW1) was below inlet 2, the air velocity at X = 1.6 m in Cases 2 and 4 was approximately 0.3 m/s, while the air velocity of Cases 1 and 3 was 0.1 m/s. In addition, the partition had little effect on the air velocity in the breathing zone of health care

worker 2 (HCW2), and the overall fluctuation was insignificant.

4.2. Temporal and spatial distributions of bioaerosols in ward

Fig. 7 shows the deposition rate, removal rate, and suspension rate of the four cases during the 900 s. The deposition rate was the ratio of the total number of deposited particles to the total number of released particles. Similarly, the ratio of the total amount of discharged particles, suspended particles, and released particles was the removal rate and suspension rate. The removal effects in Cases 1 and 3 were significantly better than those in Cases 2 and 4, which showed that unilateral downward ventilation was superior to that of bilateral downward ventilation with respect to pollutant removal. We predicted that the unidirectional flow was formed by the unilateral downward ventilation to a certain extent, while the bilateral downward ventilation created more vortices in the space, thereby hindering the effective removal of bioaerosols. The comprehensive effect of coupling flow field and thermal plume on bioaerosol removal in the ward will be studied in the follow-up work. Furthermore, the partition simultaneously caused a slight increase in the deposition rate and a slight decrease in the suspension rate of the two ventilation types.

Fig. 8 shows the temporal and spatial distributions of the bioaerosols in the four cases, and the bioaerosols are colored by particle birth time. Particle birth time indicates the time that bioaerosols are released from the breathing process so that the diffusion path of particles in the ward could be better observed. The bioaerosols moved upward along the X-wall at 160 s and continued to move toward the ceiling, as shown in the previous airflow pattern. After hitting the air supply area, the bioaerosols were divided into two portions. A small portion was diffused to the patient 2 side; however, most of the bioaerosols were diffused to the right side of patient 1 (owing to the eddy around this patient). These bioaerosols then hit the Z-wall and continued to move to the air inlet side along the wall. Affected by the eddy current on the right side of the air inlet, the bioaerosols began to spread to the entire room, as shown in Fig. 8(a), at 300 s and 500 s in Case 1. By 800 s, the bioaerosols had diffused throughout the room. The bioaerosols were blocked by the air supply area and partition in Case 3; however, a small amount of bioaerosols spread to the patient 2 side at 300 s. When separated by a partition, the number of particles on the patient 2 side at 500 s and 800 s was significantly less compared with the number of particles at the same times in Case 1.

Fig. 8(b) shows the temporal and spatial distributions of the bioaerosols in Cases 2 and 4. A portion of the bioaerosols were removed, and another portion were diffused to the right side of patient 1 along the X-wall because of the airflow. Affected by the eddy on the right side of patient 1, the bioaerosols moved upward along the corner of the room and began to spread to both sides after hitting the ceiling at 160 s in Case 2, as shown in Fig. 8(b). Then, affected by the eddy current caused by multiple air supplies, the bioaerosols continued to spread throughout the room, and they eventually spread to the entire room at 300 s, 500 s, and 800 s in Case 2, as shown in Fig. 8(b). The initial movement trajectory of the bioaerosols in Case 4 was similar to that of Case 2; however, most of the bioaerosols that diffused to the patient 2 side were held back because of the obstruction caused by the partition during the initial 180 s, only a small portion moved across the partition and the air supply area to the patient 2 side. Overall, the concentration of bioaerosols on the patient 2 side was significantly reduced compared with that of Case 2. Therefore, we concluded that the partition had a positive effect on obstructing the diffusion of bioaerosols, which was similar to the findings obtained in the study conducted by King et al. [21]. According to Qian et al. [18], downward ventilation with ceiling exhaust could be effective; however, the comparative study between downward ventilation with ceiling exhaust and these two typical downward ventilations will be discussed in the follow-up work.

In addition, by establishing a cubic area in front of the human body, the top 0.6 m × 0.6 m × 0.6 m of the cubic area was used to represent the breathing zone, and the average concentration in the cube was determined to obtain the concentration of the breathing zone with time [36]. Fig. 9 shows the average concentrations in the breathing zones of the HCWs and patient 2 at different times. The changes in the breathing zone concentrations of HCW1 during the four different cases are shown in Fig. 9(a). In the simulation process, the breathing zone concentrations in Cases 2 and 4 were almost always significantly higher than those in Cases 1 and 3, and the concentration reached approximately 10^4 CFU/m^3. The partition had little effect on the breathing zone concentration of HCW1, and the breathing zone concentration observed in Case 4 was slightly lower than that of Case 2 after 12 min, while that of Case 3 was slightly higher than that of Case 1 after 9 min. We hypothesized that the partition prevented the spread of bioaerosols in the ward, and the breathing zone concentration of HCW1 increased slightly because of the accumulation of bioaerosols on the patient 1 side.

Fig. 9(b) shows the average concentrations of the breathing zone of HCW2 at different times. The breathing zone concentrations of HCW2 were significantly lower than those of HCW1 in all four cases, and there were no obvious differences or changes in the concentrations in the four cases within 5 min. After 5 min, the breathing zone concentration of HCW2 decreased slightly with high bioaerosol removal efficiency observed in Cases 1 and 3. However, the concentration increased slightly in Cases 2 and 4 and reached approximately 10^3 CFU/m^3. The average concentrations of the breathing zone of patient 2 at different times are shown in Fig. 9(c). The concentrations in Cases 2 and 4 were still significantly higher than those of Cases 1 and 3. Therefore, the partition had a significant effect on the breathing zone concentration of patient 2. Beginning at 4 min, the concentration in Case 3 was almost always lower than the concentration in Case 1, while the concentration in Case 4 was always lower than the concentration in Case 2. This further indicated the positive effect of the partition on preventing the diffusion of bioaerosols to the patient 2 side.

4.3. Deposition characteristic of bioaerosols in ward

Surface contamination caused by pathogenic microorganisms in hospital wards poses another potential for cross-infection. Indoor microbial contaminants primarily existed in the deposition method; however, there were obvious differences in the deposition amounts and locations of the different surfaces (e.g., the walls and beds). These characteristics affected the prevention and control of contamination, as well as the cleaning and disinfection of the ward.

Fig. 10(a) and (b) show the bioaerosol deposition rates on the indoor walls, beds, and body surfaces during 15 min for the four cases. The deposition rate was calculated as the ratio of the deposited bioaerosol amount on every surface to the total amount of bioaerosol released. The bioaerosols in Case 1 were primarily deposited on patient 1, bed 1, and the X-wall with deposition rates of 1.74%, 2.04%, and 4.9%, respectively. Combined with previous analysis, the main diffusion path of the bioaerosols occurred along the path of the airflow; therefore, the bioaerosols were mainly deposited on the X-wall. The backflow formed after the airflow moved to the ceiling and caused a portion of the bioaerosols to be deposited on the surfaces of patient 1 and bed 1.

The deposition rate on the X-wall in Case 3 (5.82%) was slightly higher than the rate determined in Case 1. The deposition on the surfaces of HCW1 and the ceiling increased slightly, which was because the partition blocked the diffusion of the bioaerosol particles to the patient 2 side. With an increase in the concentration of particles on the patient 1 side, the deposition on each of the surfaces increased as well.

In Case 2, the bioaerosols were primarily deposited on the X-wall, which was because of the eddy current formed by the airflow that hit the wall. Bioaerosols accumulated in the corner formed by the X- and Z-walls; they then moved upward and gradually diffused to the entire ward. Several of the bioaerosols spread outward along the X-wall, resulting in a deposition rate of 15.4% on the X-wall and to varying degrees on the ceiling, floor, and Z-wall.

The amounts of deposition on the ceiling and X-wall in Case 4 also increased, which was similar to the conclusion obtained Case 1 and Case 3, and the deposition ratios were 19.1% and 5.29%, respectively. Similarly, the deposition rate of bioaerosols on the other surfaces decreased to varying degrees during the 900 s.

In summary, the main deposition locations in the ward for the four cases were near the head of patient 1. The eddy current area generated by the downward ventilation was mostly near the wall on the same side of the room as the patient's head. Additional hospital research has shown that a bedside table is a high-frequency contact point for HCWs [37], which also proved that the probability of contact transmission is at least 20% [38]. Thus, these locations require more attention and study.

5. Conclusion

This study provided a comparison between full-scale experimental bioaerosol deposition and CFD simulation against cross-infection in a two-bed hospital ward. The validity of the CFD simulation was verified by consistent experimental results. The effectiveness of bioaerosol removal and the protective effect on HCWs and nearby patients were examined and discussed for four different cases. The main conclusions were as follows.

1) The removal effect of bioaerosols in cases with unilateral downward ventilation was better than that of bilateral downward ventilation. The removal rates of bioaerosols in wards with unilateral downward ventilation were 82.96% (Case 1) and 82.97% (Case 3), while those of wards with bilateral downward ventilation were 32.15% (Case 2) and 32.86% (Case 4). Compared with that of bilateral downward ventilation, patient 2 and the HCWs had a lower time-average breathing zone concentration in the ward with unilateral downward ventilation.
2) A partition had a positive effect on protecting the patient on the other side of it in the same ward. The bioaerosol concentration on the patient 2 side was significantly reduced in the two cases with a partition; thus, the breathing zone concentration of patient 2 was significantly reduced. However, no obvious protective effect was observed with respect to the HCWs. Meanwhile, a partition could reduce the deposition of microbial aerosols on most surfaces. Therefore, the addition of a partition between hospital beds may reduce the risk of transmission between patients after the release of bioaerosols from adjacent patients; however, it is necessary that HCWs still protect themselves properly.
3) The main deposition locations in the ward with the two downward ventilation types were near the wall on the same side of the room as the patient's head. In the ward with bilateral downward ventilation, nearly 35% of the bioaerosol was deposited on the walls, while only 10% was deposited on the walls in the ward with unilateral downward ventilation. The wall near the eddy current area was the most significant area of deposition. Therefore, to a certain extent, maintaining the frequency of cleaning and disinfection of high-frequency contact areas is effective in reducing indirect transmission.

Declaration of competing interest

The author(s) declared no potential conflicts of interest with respect to the research, authorship, and/or publication of this article.

Acknowledgement

This work was supported by the National Natural Science Foundation of China (No.41977368 and No.51708211), the Opening Funds of State Key Laboratory of Building Safety and Built Environment National Engineering Research Center of Building Technology (BSBE2017-08), Natural Science Foundation of Hebei Province (No. E2017502051) and the Fundamental Research Funds for the Central Universities (No.2018MS103 and No.2020YJ007).

References

[1] E.A. Hathway, C.J. Noakes, P.A. Sleigh, L.A. Fletcher, CFD simulation of airborne pathogen transport due to human activities, Build. Environ. 46 (12) (2011) 2500–2511, https://doi.org/10.1016/j.buildenv.2011.06.001.
[2] C. He, I.M. Mackay, K. Ramsay, Z. Liang, T. Kidd, L.D. Knibbs, G. Johnson, D. McNeale, R. Stockwell, M.G. Coulthard, D.A. Long, T.J. Williams, C. Duchaine, N. Smith, C. Wainwright, L. Morawska, Particle and bioaerosol characteristics in a paediatric intensive care unit, Environ. Int. 107 (2017) 89–99, https://doi.org/10.1016/j.envint.2017.06.020.
[3] J.C. Luongo, K.P. Fennelly, J.A. Keen, Z.J. Zhai, B.W. Jones, S.L. Miller, Role of mechanical ventilation in the airborne transmission of infectious agents in buildings, Indoor Air 26 (5) (2016) 666–678, https://doi.org/10.1111/ina.12267.
[4] J. Cho, Investigation on the contaminant distribution with improved ventilation system in hospital isolation rooms: effect of supply and exhaust air diffuser configurations, Appl. Therm. Eng. 148 (2019) 208–218, https://doi.org/10.1016/j.applthermaleng.2018.11.023.
[5] CDC, Guidelines for preventing the transmission of mycobacterium tuberculosis in health-care settings, Morb. Mortal. Wkly. Rep. 54 (RR17) (2005), 1 141.
[6] J.W. Tang, C.J. Noakes, P.V. Nielsen, I. Eames, A. Nicolle, Y. Li, G.S. Settles, Observing and quantifying airflows in the infection control of aerosol- and airborne-transmitted diseases: an overview of approaches, J. Hosp. Infect. 77 (3) (2011) 213–222, https://doi.org/10.1016/j.jhin.2010.09.037.
[7] H. Brohus, P.V. Nielsen, Dispersal of exhaled air and personal exposure in displacement ventilated rooms, Indoor Air 12 (3) (2010) 147–164, https://doi.org/10.1034/j.1600-0668.2002.08126.x.
[8] L. Morawska, Droplet fate in indoor environments, or can we prevent the spread of infection? Indoor Air 16 (5) (2006) 335–347, https://doi.org/10.1111/j.1600-0668.2006.00432.x.
[9] Y. Li, S. Duan, I.T. Yu, T.W. Wong, Multi-zone modeling of probable SARS virus transmission by airflow between flats in Block E, Amoy Gardens, Indoor Air 15 (2) (2005) 96–111, https://doi.org/10.1111/j.1600-0668.2004.00318.x.
[10] T.S. Yu, W.T. Wai, C.Y. Lan, L. Nelson, Y. Li, Temporal-spatial analysis of severe acute respiratory syndrome among hospital inpatients, Clin. Infect. Dis. (9) (2005) 1237–1243, https://doi.org/10.1086/428735.
[11] K.W.D. Cheong, S.Y. Phua, Development of ventilation design strategy for effective removal of pollutant in the isolation room of a hospital, Build. Environ. 41 (9) (2006) 1161–1170, https://doi.org/10.1016/j.buildenv.2005.05.007.
[12] T. Lim, J. Cho, B.S. Kim, The predictions of infection risk of indoor airborne transmission of diseases in high-rise hospitals: tracer gas simulation, Energy Build. 42 (8) (2010) 1172–1181, https://doi.org/10.1016/j.enbuild.2010.02.008.
[13] Y.C. Tung, Y.C. Shih, S.C. Hu, Numerical study on the dispersion of airborne contaminants from an isolation room in the case of door opening, Appl. Therm. Eng. 29 (8) (2009) 1544–1551, https://doi.org/10.1016/j.applthermaleng.2008.07.009.
[14] S.H. Ho, L. Rosario, M.M. Rahman, Three-dimensional analysis for hospital operating room thermal comfort and contaminant removal, Appl. Therm. Eng. 29 (10) (2009) 2080–2092, https://doi.org/10.1016/j.applthermaleng.2008.10.016.
[15] P.V. Nielsen, Y. Li, M. Buus, F.V. Winther, Risk of cross-infection in a hospital ward with downward ventilation, Build. Environ. 45 (9) (2010) 2008–2014, https://doi.org/10.1016/j.buildenv.2010.02.017.
[16] H. Qian, Y. Li, P.V. Nielsen, C.E. Hyldgaard, T.W. Wong, A.T. Chwang, Dispersion of exhaled droplet nuclei in a two-bed hospital ward with three different ventilation systems, Indoor Air 16 (2) (2006) 111–128, https://doi.org/10.1111/j.1600-0668.2005.00407.x.
[17] Y. Yin, W. Xu, J. Gupta, A. Guity, P. Marmion, A. Manning, B. Gulick, X. Zhang, Q. Chen, Experimental study on displacement and mixing ventilation systems for a patient ward, HVAC R Res. 15 (6) (2009) 1175–1191, https://doi.org/10.1080/10789669.2009.10390885.
[18] H. Qian, Y. Li, P.V. Nielsen, C.E. Hyldgaard, Dispersion of exhalation pollutants in a two-bed hospital ward with a downward ventilation system, Build. Environ. 43 (3) (2008) 344–354, https://doi.org/10.1016/j.buildenv.2006.03.025.
[19] A.C.K. Lai, F. Chen, Modeling particle deposition and distribution in a chamber with a two-equation Reynolds-averaged Navier–Stokes model, J. Aerosol Sci. 37 (12) (2006) 1770–1780, https://doi.org/10.1016/j.jaerosci.2006.06.008.
[20] Q. Chen, Z. Jiang, A. Moser, Control of airborne particle concentration and draught risk in an operating room, Indoor Air 2 (3) (1992) 154–167, https://doi.org/10.1111/j.1600-0668.1992.04-23.x.
[21] M.F. King, C.J. Noakes, P.A. Sleigh, M.A. Camargo-Valero, Bioaerosol deposition in single and two-bed hospital rooms: a numerical and experimental study, Build, Environ. Times 59 (2013) 436–447, https://doi.org/10.1016/j.buildenv.2012.09.011.
[22] C. Xu, X. Wei, L. Liu, L. Su, P.V. Nielsen, Effects of personalized ventilation interventions on airborne infection risk and transmission between occupants, Build. Environ. 180 (2020) 107008, https://doi.org/10.1016/j.buildenv.2020.107008.
[23] V.L. Gillespie, C.S. Clark, H.S. Bjornson, S.J. Samuels, J.W. Holland, A comparison of two-stage and six-stage Andersen impactors for viable aerosols, Am. Ind. Hyg. Assoc. J. 42 (12) (1981) 858–864, https://doi.org/10.1080/15298668191420819.
[24] Z. Fang, Z. Ouyang, H. Zheng, X. Wang, Concentration and size distribution of culturable airborne microorganisms in outdoor environments in Beijing, China, Aerosol Sci. Technol. 42 (5) (2008) 325–334, https://doi.org/10.1080/02786820802068657.

[25] J.I. Choi, J.R. Edwards, Large-eddy simulation of human-induced contaminant transport in room compartments, Indoor Air 22 (1) (2012) 77–87, https://doi.org/10.1111/j.1600-0668.2011.00741.x.
[26] C. Wang, S. Holmberg, S. Sadrizadeh, Numerical study of temperature-controlled airflow in comparison with turbulent mixing and laminar airflow for operating room ventilation, Build. Environ. 144 (2018) 45–56, https://doi.org/10.1016/j.buildenv.2018.08.010.
[27] Q. Chen, Comparison of different k-ε models for indoor air flow computations, Numer Heat Tranf. B-Fundam. 28 (3) (1995) 353–369, https://doi.org/10.1080/10407799508928838.
[28] B. Eliseo, G.-D. Fernando-Juan, C. Salvador, T. Antonio, H. Antonio, Measurement and numerical simulation of air velocity in a tunnel-ventilated Broiler house, Sustainability 7 (2) (2015) 2066–2085, https://doi.org/10.3390/su7022066.
[29] E. Küçüktopcu, B. Cemek, Evaluating the influence of turbulence models used in computational fluid dynamics for the prediction of airflows inside poultry houses, Biosyst. Eng. 183 (2019) 1–12, https://doi.org/10.1016/j.biosystemseng.2019.04.009.
[30] B. Zhao, Y. Zhang, X. Li, X. Yang, D. Huang, Comparison of indoor aerosol particle concentration and deposition in different ventilated rooms by numerical method, Build. Environ. 39 (1) (2004) 1–8, https://doi.org/10.1016/j.buildenv.2003.08.002.
[31] Hinds, Aerosol Technology: Properties, Behavior, and Measurement of Airborne Particles, Wiley, 1982.
[32] J. Wei, Y. Li, Enhanced spread of expiratory droplets by turbulence in a cough jet, Build. Environ. 93 (2015) 86–96, https://doi.org/10.1016/j.buildenv.2015.06.018.
[33] P.V. Nielsen, F. Allard, H.B. Awbi, et al., CFD in Ventilation Design a New REHVA Guide Book, Aalborg University, 2009.
[34] Y. Li, X. Huang, I.T.S. Yu, T.W. Wong, H. Qian, Role of air distribution in SARS transmission during the largest nosocomial outbreak in Hong Kong, Indoor Air 15 (2) (2005) 83–95, https://doi.org/10.1111/j.1600-0668.2004.00317.x.
[35] F. Romano, L. Marocco, J. Gustén, C.M. Joppolo, Numerical and experimental analysis of airborne particles control in an operating theater, Build. Environ. 89 (2015) 369–379, https://doi.org/10.1016/j.buildenv.2015.03.003.
[36] Y. Tao, K. Inthavong, J.Y. Tu, Dynamic meshing modelling for particle resuspension caused by swinging manikin motion, Build. Environ. 123 (2017) 529–542, https://doi.org/10.1016/j.buildenv.2017.07.026.
[37] K. Huslage, W.A. Rutala, E.E. Sickbertbennett, D.J. Weber, A quantitative approach to defining "high-touch" surfaces in hospitals, Infect. Control Hosp. Epidemiol. 31 (8) (2010) 850–853, https://doi.org/10.1086/655016.
[38] M.K. Hayden, D.W. Blom, E.A. Lyle, C.G. Moore, R.A. Weinstein, Risk of hand or glove contamination after contact with patients colonized with vancomycin-resistant enterococcus or the colonized patients' environment, Infect. Control Hosp. Epidemiol. 29 (2) (2008) 149–154, https://doi.org/10.1086/524331.